

Silicon Nano-membranes for Efficient Large Angle Optical Beam Steering

Amir Hosseini, *Student Member, IEEE*, Yang Zhao, *Student Member, IEEE*,
Yun-Sheng Chen, *Student Member, IEEE*, David N. Kwong, and Ray T. Chen, *Fellow, IEEE*
Microelectronics Research Center, Electrical and Computer Engineering Department,
the University of Texas at Austin, Austin, TX 78758

Abstract—In this paper, we present a silicon nano-membrane-based phased array structure for large angle optical beam steering. The new array structure allows for over $\pm 60^\circ$ optical beam scanning with minimal degradation in the side-lobe-level and diffraction efficiency.

Optical phased arrays (OPAs) represent an enabling technology that makes possible simple, affordable, and lightweight laser beam steering with very precise stabilization, random-access pointing and programmable multiple simultaneous beams [1]. In the past decades, optical beam steering has been achieved through mechanically controlled MEMs system and liquid crystal-based optical phased array [1], [2].

However, both of these systems suffer from low steering speed and limited steering angle. GHz steering speed phased array optical beam steering has been reported recently by [3]. But only about 6° steering angle is achieved. To achieve a large steering angle without introducing grating lobes, J.Abeles and R. Deri [4] proposed unequally spaced waveguide arrays to suppress the side lobes in the far-field pattern. However, the study did not include a design procedure to minimize the grating lobes. This idea was adopted by [5], [6], where the spacing between the radiators in the array is set either randomly or by an optimization process. Here, we report a technique to suppress the grating lobes for large angle beam steering up to $\pm 60^\circ$, and discuss the maximum performance achievable by un-equally spaced OPAs.

A schematic of a silicon nano-membrane-based OPA system is shown in Figure 1 (a). Similar to their microwave counterparts, linear optical phased arrays consists of 1D or 2D arrays of N single-mode waveguides operating at the designated wavelengths. The far-field pattern associated with the array factor is given as $\sum_n e^{j\vec{k}\cdot\vec{d}_n}$, where, $\vec{k} = k\hat{r}$, $k = \frac{2\pi}{\lambda}$, \vec{d}_n is the translational vector of the n^{th} radiator position and λ is the wavelength. In the case of 1D linearly phased arrays in the Y -direction as shown in Figures 1(b) and (c), $\vec{k}\cdot\vec{d}_n = \frac{2\pi d_n}{\lambda} \sin \phi + \beta_n$, where β_n is the phase shift imposed on the n^{th} radiator and β_n/d_n is constant. Beam steering can be done by changing the linear phase shift imposed on the array. However the maximum grating lobe-free steering angle is limited. We consider the far field pattern for an individual radiator as $EF(\phi) = \frac{\sin(\frac{\pi}{\lambda} \sin \phi)}{(\frac{\pi}{\lambda} \sin \phi)}$, $\lambda = 1550 \text{ nm}$ and the aperture size in the Y -direction $a = 500 \text{ nm}$, which is to insure single-mode operation.

Consider the radiation patterns for two uniform arrays with

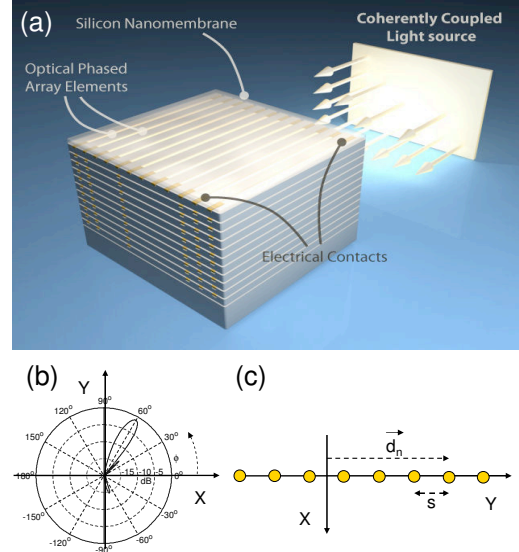


Fig. 1. (a) A schematic of silicon nano-membrane-based OPA beam steering. (b) Radiation pattern for uniform array ($N = 16$) with $d_{n+1} = d_n = s = \lambda/2$ and $\beta_{n+1} - \beta_n = \Delta\beta = 156^\circ$. (c) A uniform array structure.

spacings $s = 3\lambda/2$ and $s = 2\lambda$, where $\beta_n = 0$ [Figure 1(c)]. In both cases, the existence of the grating lobes increases the side-lobe-level (SLL), defined as the ratio of the second largest lobe intensity to the maximum intensity (main lobe) [7]. We notice that the grating lobes in the two cases happen for $\phi = \pm \sin^{-1} \frac{2}{3}$ and $\phi = \pm \sin^{-1} \frac{1}{2}$, $\pm \sin^{-1} 1$, for $s = 3\lambda/2$ and $s = 2\lambda$, respectively and they do not overlap. However, the main lobes (ϕ_0) in both cases occur at $\sin \phi_0 = \frac{\lambda}{2\pi} \frac{\beta_n}{d_n}$, which will be the same, for all the steering angles, as long as the condition $\frac{\beta_n}{d_n} = \text{constant}$ is satisfied.

An un-equally spaced OPA is shown in Figure 2(a). There are M sub-arrays with different spacing (s_m) between adjacent radiators, where, $s_m = q_m s_0$, and s_0 is a design parameter. The number of radiators in each sub-array is N/M , where N is the total number of radiators. The radiation pattern for $M = 2$, $s_1 = 3s_0$, $s_2 = 4s_0$ and $s_0 = \lambda/2$ is shown in Figure 2(b). The constructive interference at the main lobe and avoiding constructive interference at grating lobes, result in $SLL = -6\text{dB}$.

Increasing the number of radiators while keeping the number of sub-arrays constant results in narrower beam widths,

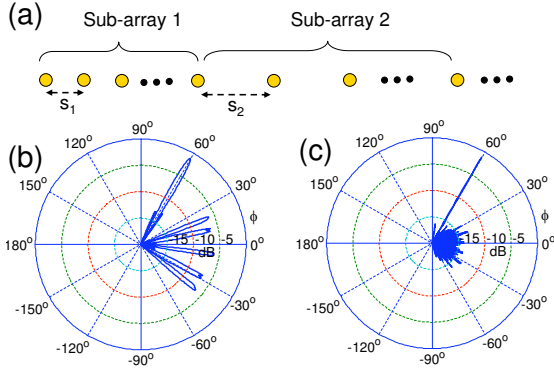


Fig. 2. (a) A schematic of the presented un-equally spaced OPA structure. Radiation pattern for (b) $M=2$ and $N=16$ and (c) $M=6$, $N=96$.

but does not decrease the SLL . However, doubling M can further suppress the grating lobe by 6dB . In order to avoid overlaps between the grating lobe of different sub-arrays, q_m values should not have common factors numerically. In order to reduce the number of grating lobes, and therefore, energy loss due to radiation in any direction rather than the main lobe [high diffraction efficiency (η)], one may consider $q_1 = 3$, $q_2 = 4$, $q_3 = 5$, $q_4 = 7$, $q_5 = 11$, $q_6 = 13$, ... Figure 2(c) shows the radiation pattern for $M = 6$, $N = 96$, $s_0 = \lambda/2$ and $\phi_0 = 0^\circ$, 60° .

Variation of SLL with N is demonstrated in Figure 3(a) for different M and ϕ values. For $M \geq 2$, SLL values decreases with N and saturate at $-20 \log M$. Due to the overlap of more grating lobes associated with each sub-array, SLL may be larger for small N and large M values. As the grating lobes become narrower with increasing N , the overlap between the adjacent grating lobes of different sub-arrays significantly reduces, and consequently SLL decreases.

Another important figure of merit is the diffraction efficiency η defined as $\frac{A_0^2}{\sum_{i=0} A_i^2}$, where, A_0 is the main lobe and A_i for $i \geq 1$ are the grating lobes. Figure 3(b) shows the variation of η with N for different M and ϕ values. Figures 3 (c) and (d) demonstrate the variation of SLL and η versus N for $M = 4$ and $s_0 = 0.5\lambda$, 0.3λ and 0.1λ . For a fair comparison in the context of manufacturability, we have considered $[q_1, q_2, q_3, q_4] = [3, 4, 5, 7]$, $[5, 6, 7, 11]$ and $[15, 16, 17, 19]$ for $s_0 = 0.5\lambda$, 0.3λ and 0.1λ , respectively, so that the minimum spacing between the array elements become $s_1 = q_1 s_0 = 1.5\lambda \approx 4600 \text{ nm}$. Since SLL is a function of M in $OPAs$, the SLL values for the three cases are almost the same. However, for large enough N , efficiency is higher for smaller s_0 values. Figures 3(b) and (d) indicate that silicon nano-membrane-based OPA structure allows for $\eta > 30\%$ at $\phi_0 = 60^\circ$. Note that in the case of an ideal liquid crystal-based OPA, η drops to 30% at $\phi_0 \approx 40^\circ$ (for $\lambda = 1550 \text{ nm}$), but in practice, fringing electric fields and limited liquid crystal birefringence severely degrade the diffraction efficiency [8].

For research purposes, we are going to use Raith 50 electron beam lithography system to pattern the ridge waveguide structures directly on a SOI wafer with 250 nm silicon membrane

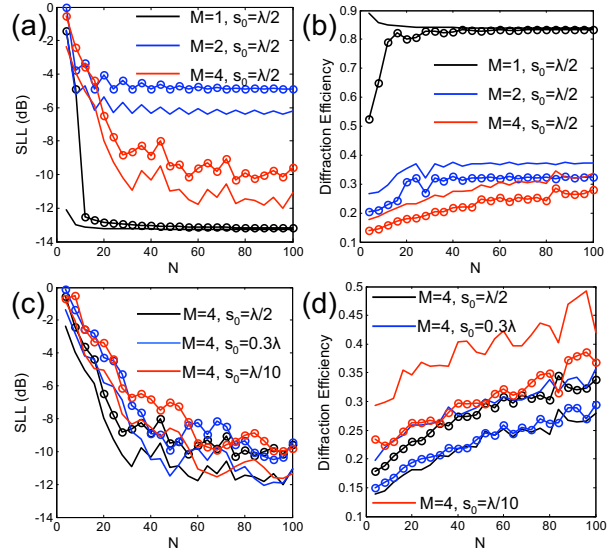


Fig. 3. Variation of SLL and diffraction efficiency with N at $\phi_0 = 0^\circ$ (solid lines) and $\phi_0 = 60^\circ$ (circles) for (a) and (b) $s_0 = \lambda/2$ and different M values (c) and (d) for $M = 4$ and different s_0 values.

on top of a 3000 nm buried oxide layer. The ridge width is 450 nm and height is 200 nm to allow single mode propagation at 1550 nm wavelength. A reactive ion etching process follows the lithography process will be performed on a $790 \text{ Plasma Therm RIE}$ etcher, and the etching roughness and fabricated ridge height will be observed under a Digital Instruments AFM Series IV atomic force microscope.

In conclusion, we presented an OPA design technique for efficient and low SLL large beam steering in the optical region while relaxing the requirement of small spacing ($\lambda/2 \approx 800 \text{ nm}$), which in the case of the conventional OPA structures results in fabrication difficulties and optical coupling between adjacent waveguides. The detailed fabrication and measurement data will be presented at the conference.

This research is supported by the multi-disciplinary university research initiative (MURI) program through the AFOSR.

REFERENCES

- [1] P. McManamon, T. Dorschner, D. Corkum, L. Friedman, D. Hobbs, M. Holz, S. Liberman, H. Nguyen, D. Resler, R. Sharp, and E. Watson, "Optical phased array technology," *Proceedings of the IEEE*, vol. 84, no. 2, pp. 268–298, 1996.
- [2] P. McManamon, "An overview of optical phased array technology and status," *Proc. SPIE*, vol. 5947, no. 593701, 2005.
- [3] R. F. P. M. Jarrahi, D. A. Miller, and T. H. Lee, "An overview of optical phased array technology and status," *Applied Physics Letters*, vol. 92, no. 014106, 2008.
- [4] J. H. Abeles and R. J. Deri, "Suppression of sidelobes in the far-field radiation patterns of optical waveguide arrays," *Applied Physics Letters*, vol. 53, no. 15, 1988.
- [5] F. Xiao, W. Hu, and A. S. Xu, "Optical phased-array beam steering controlled by wavelength," *Applied Optics*, vol. 44, no. 26, pp. 5429–543, 2005.
- [6] F. Xiao, G. Li, Y. Li, and A. Xu, "Fabrication of irregular optical phased arrays on silicon-on-insulator wafers," *Optical Engineering*, vol. 47, no. 4, p. 040503, 2008.
- [7] R. J. Mailloux, *Phased Array Antenna Handbook*. Artech House, 1993.
- [8] X. Wang, B. Wang, P. J. Bos, P. F. McManamon, J. J. Pouch, F. A. Miranda, and J. E. Anderson, "Modeling and design of an optimized liquid-crystal optical phased array," *Journal of Applied Physics*, vol. 98, no. 7, p. 073101, 2005.